Extremely weak Lg attenuation reveals ancient continental relicts in the South China block

Lin Shen [a,b], Lian-Feng Zhao [a,c,*], Xiao-Bi Xie [d], Geng Yang [a,b], Zhen-Xing Yao [a]

[a] *Key Laboratory of Earth and Planetary Physics, Institute of Geology and Geophysics, Chinese Academy of Sciences, Beijing, China*
[b] *College of Earth and Planetary Sciences, University of Chinese Academy of Sciences, Beijing, China*
[c] *Heilongjiang Mohe Observatory of Geophysics, Institute of Geology and Geophysics, Chinese Academy of Sciences, Beijing, China*
[d] *Institute of Geophysics and Planetary Physics, University of California at Santa Cruz, CA 95064, USA*

ARTICLE INFO

ABSTRACT

Whether the South China block (SCB) occupied an external or internal position in the Rodinia supercontinent remains controversial. The external model favors an accretion orogenic amalgamation setting, whereas the internal model assumes postcollisional extensional rifting in the Neoproterozoic. Recent geochronological data suggested that the SCB was assembled from several ancient nuclei or microcontinental fragments with various origins and geological histories during the early Neoproterozoic, and supported the external position model for the SCB in Rodinia. However, whether these ancient continental nuclei are hidden in the crust requires direct constraints such as those from seismic tomography. In general, these early ancient continental relicts preserved in the present-day crust tend to be characterized by high strength, high velocity, and weak attenuation. Compared with velocity, seismic attenuation tends to be more sensitive to ancient rigid continental fragments. Here, we constructed a high-resolution broadband crustal Lg attenuation model for the SCB and explored the existence and scale of the ancient continental fragments potentially hidden in the deep crust. Four extremely weak attenuation anomalies in the SCB indicate potential locations of these ancient continental relicts in the crust; one is in the Sichuan basin and the other three are beneath the Cathaysia block. The three ancient continental relicts in the Cathaysia block, which are closely corresponding to early surface lithological records, provide seismic evidence supporting an external position for the SCB in the Rodinia supercontinent.

© 2023 Elsevier B.V. All rights reserved.

1. Introduction

The Archean continental nuclei originated from oceanic plateaus formed by mantle plumes or island arcs via oceanic subduction (e.g., Zhu et al., 2021). These Archean continental nuclei grew under the intra-oceanic and continental margin arc systems and formed the present unified continents (e.g., Kusky and Wang, 2022). However, the unified block may also have been broken up along continental rifting areas due to intense extension (e.g., Brune et al., 2022). For example, eastern Africa may split into a nascent microcontinent or continental nuclei along the continental rifting system in the future, where these microcontinents may share similar geological records (Biggs et al., 2021). For the SCB, several ancient continental nuclei or microcontinental fragments have been recognized from geochronology data (e.g., Shu et al., 2021; Yu et al., 2010). It is speculated that they were derived from fragment amalgamation along the margin of Rodinia with different early tectonic records (Cawood et al., 2017; Wang et al., 2014; Yao et al., 2017) or breakup from the early Rodinia supercontinent sharing a similar tectonic evolution and recording common tectono-thermal events (Li et al., 2002; Shu, 2006). These ancient continental nuclei are sometimes difficult to destroy; thus, they might be preserved as relict continental fragments underlying the modern crust (e.g., Lee et al., 2011). Combining surface geological data and deep phys-

ical properties from geophysical observations can help us refine these ancient continental relicts from the current associations and provide further constraints to trace early tectonic activities in the SCB (e.g., Cawood et al., 2020).

The SCB, located in the southeastern part of the Eurasia continent, consists of the Yangtze Craton and the Cathaysia block, and these two blocks were consolidated along the Jiangnan orogen during the Neoproterozoic (Fig. 1a) (e.g., Wang et al., 2013; Zhao and Cawood, 2012). Due to intense orogenesis and magmatism by Paleo-Pacific subduction during the Mesozoic, the SCB is covered by widespread igneous rocks with sparse Precambrian outcrops (Fig. 1b). Previous studies on detrital and xenocrystal zircons suggested that several Archean continental fragments with various origins and distinct geological histories exist in the SCB crust, indicating the SCB may be located along the margin of the Rodinia supercontinent (e.g., Cawood et al., 2017; Wang et al., 2014; Yu et al., 2010). Based on the detrital zircon data, Yu et al. (2010) considered that the Cathaysia block was divided into two distinct ancient nuclei or microcontinents during the Neoproterozoic, i.e., the Wuyishan terrane to the northwest and the Nanling-Yunkai terrane to the southwest. Shu et al. (2021) divided the Cathaysia block into three ancient continental fragments named the Wuyishan, Nanling, and Yunkai terranes based on their ages and compositional characteristics; the Wuyishan terrane is the oldest, and the Nanling and Yunkai terranes have similar ages. They speculated that the Cathaysia block formed by westward expansion from the Wuyishan nucleus to the Nanling and Yunkai terranes during the Neoproterozoic. Therefore, whether these ancient continental nuclei exist in the Cathaysia block and their potential distributions in the current deep crust need more constraints from geophysical observations.

After multiple tectonic evolution stages, these ancient continental nuclei may remain in the deep crust and be characterized by low tectonic activity, high strength, low temperature, and hence high seismic velocity and low seismic attenuation (e.g., Fan and Lay, 2002; Paul and Ghosh, 2019). Therefore, seismic tomography can be effective in investigating potential ancient continental nuclei. For example, the S-wave velocity tomography imaged a high-velocity zone in the western part of the Yangtze Craton, probably indicating the location of an ancient continental nucleus in the deep crust (e.g., Zhou et al., 2012). However, it is difficult to depict the ancient continental fragments in the Cathaysia block against a high-velocity background, even with a high-resolution velocity tomography (e.g., Zhou et al., 2012). Compared with seismic velocity, seismic attenuation reflects the anelasticity and scattering properties of the Earth's interior, is more sensitive to the rheological strength, and can provide effective constraint on the distribution of ancient continental relicts (e.g., Kampfmann and Berckhemer, 1985; Mitchell, 1995). For instance, Chen and Xie (2017) developed an 1.0 Hz Lg-wave attenuation model for the SCB, found that the Wuyishan terrane is characterized by weak attenuation, and suggested that there may exist the Precambrian basement.

Lg-wave is the most prominent seismic phase in regional seismograms and can be considered as the superposition of supercritically reflected shear waves or a sum of high-mode surface waves in the crustal waveguide (e.g., Kennett, 1986; Knopoff et al., 1973). By sampling the continental crust, the Lg-wave amplitude decay can measure the crustal attenuation and to infer the thermal status, the scattering effect and rheological strength (e.g., He et al., 2021). The Lg-wave attenuation can be quantified by the dimensionless quality factor Q_{Lg}, which denotes the fractional energy loss per cycle (e.g., Phillips et al., 2005). In general, an old, cold, rigid, and stable geoblock tends to be characterized by high Q (weak attenuation), whereas a younger, hotter, softer, and active geoblock often has low Q (strong attenuation) (e.g., Fan and Lay, 2002; Mitchell and Hwang, 1987). However, limited by the available data, previous Q_{Lg} results often have low resolution and in a narrow frequency

band near 1.0 Hz (Chen and Xie, 2017; Hearn et al., 2008; Phillips et al., 2005). In this study, benefited from the dense broadband network and data accumulated during the last couple of decades, we developed a high-resolution broadband Lg attenuation model for the SCB and surrounding areas. The Q_{Lg} frequency dependency is highly complex. Both the intrinsic and scattering mechanisms contribute to the attenuation, and both are frequency dependent (e.g., Sato et al., 2012; Wu et al., 2000). More important, the Lg-wave propagation is highly affected by the waveguide structure, including the reflectivity and roughness of the free surface and the Moho discontinuity, sudden change of the crust thickness, etc (e.g., Zhang and Lay, 1995). Lg waves of different modes can couple with each other or even be blocked. All these are frequency dependent phenomena. Therefore, the Q_{Lg} is not simply a medium Q, instead, it is an apparent Q mixed the frequency dependencies from the medium and the waveguide structure. Under this circumstance, investigating the Lg attenuation in a broadband can provide more constrains on the property and structure of the underlying processes than just using a narrow band Q (e.g., He et al., 2021; Wu et al., 2000; Zhao et al., 2013). In this study, we will combine lateral variations of broadband Lg attenuation in the study region with other geological, geophysical, and geochronological data, to explore the distribution of potential ancient continental relicts underlying the SCB.

2. Data and method

We collected 59, 811 broadband vertical component seismograms generated by 218 crustal earthquakes that occurred in the SCB and surrounding areas between January 2000 and November 2018 with epicentral distances (i.e., the distance from the earthquake to the seismic station) ranging from 200 to 3000 km. These seismograms were recorded by 580 regional broadband seismic stations, which included 44 stations from the Incorporated Research Institutions for Seismology (IRIS) Data Management Center and 536 stations from the China Earthquake Network Center (CENC) (Figs. 1a, S1). All earthquakes used in this study occurred within the crust with focal depths shallower than the Moho discontinuity given by the CRUST 1.0 model (Laske et al., 2013). To guarantee the quality of observed Lg-waves and avoid the effect from large earthquake rupture, we chose earthquakes with their magnitudes between 3.5 and 6.0 (e.g., Zhao et al., 2013). To obtain better seismic ray coverage, we attempted to select earthquakes as evenly distributed as possible. We also required that each station recorded at least three events and each event was recorded by at least three stations to ensure sufficient constraints on the source function and site response (e.g., Zhao and Xie, 2016). As an example, Fig. 2a illustrates selected seismograms from an earthquake that occurred in the Sichuan Basin.

The data preprocessing was conducted following the procedure proposed by Zhao et al. (2013). First, the Lg waveform was extracted using a group velocity window between 3.6 and 3.0 km/s. We also applied time windows of the same length before the first P-wave and Lg-wave to pick the pre-event and pre-Lg noise. Cosine tapers of 10% window length were added to both ends of these time windows, followed by calculating the Fourier spectra of the Lg-wave, and pre-event and pre-Lg noises (Figs. 2b and 2c). To obtain the broadband Q_{Lg} model, the Lg-wave and noise spectral amplitudes were sampled at 58 reference frequencies log-evenly distributed between 0.05 and 10 Hz. Then, the signal-to-noise ratios (SNR) for both the pre-event and pre-Lg noise (Figs. 2d and 2e) were calculated at individual frequencies. The Lg amplitudes with pre-event SNR higher than 2.0 and pre-Lg SNR higher than 1.0 were selected (e.g., He et al., 2021). These SNR thresholds can ensure the Lg data quality and remove data potentially dominated by the Sn coda. Assuming the seismic record is composed of both
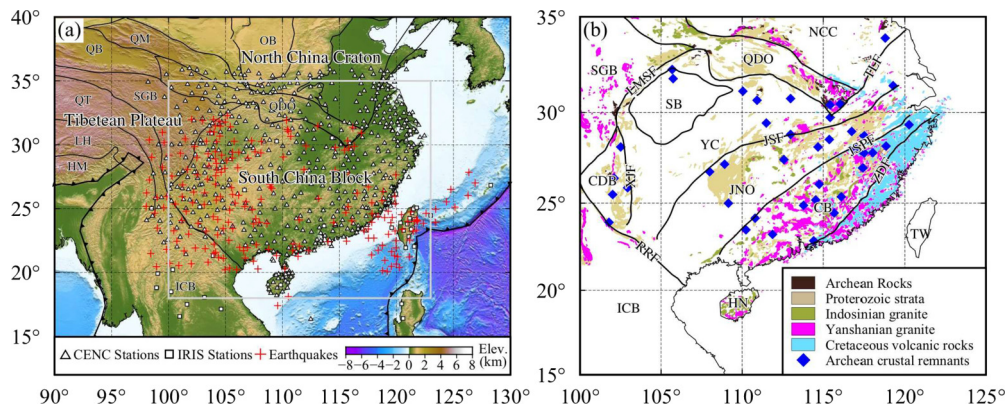
Fig. 1. (a) Topographic map showing the southeastern margin of the Eurasian continent. The superimposed are major block boundaries (black lines), seismic stations from the China Earthquake Network Center (CENC) (triangles) and Incorporated Research Institutions for Seismology (IRIS) (squares), and earthquakes for Q_{Lg} estimation (red crosses). The study region is shown by the gray rectangle. (b) Distribution of rocks from several typical stages in the SCB and surrounding areas (Ye et al., 2017). The Archean crustal remnants identified by zircon U–Pb ages are taken from Zhang and Zheng (2013). The abbreviations are CB, Cathaysia block; CDB, Chuandian block; HM, Himalaya block; HN, Hainan Island; ICB, Indo-China block; JNO, Jiangnan orogen; JSF, Jiujiang-Shitai buried fault; JSPF, Jiangshan-Shaoxing-Pingxiang fault; LH, Lhasa block; LMSF, Longmenshan fault; NCC, North China Craton; OB, Ordos Basin; QB, Qaidam Basin; QDO, Qinling-Dabie orogen; QM, Qilian Mountains; QT, Qiangtang block; RRF, Red River fault; SB, Sichuan Basin; SGB, Songpan-Ganzi block; TW, Taiwan; YC, Yangtze Craton; ZDF, Zhenghe-Dapu fault.
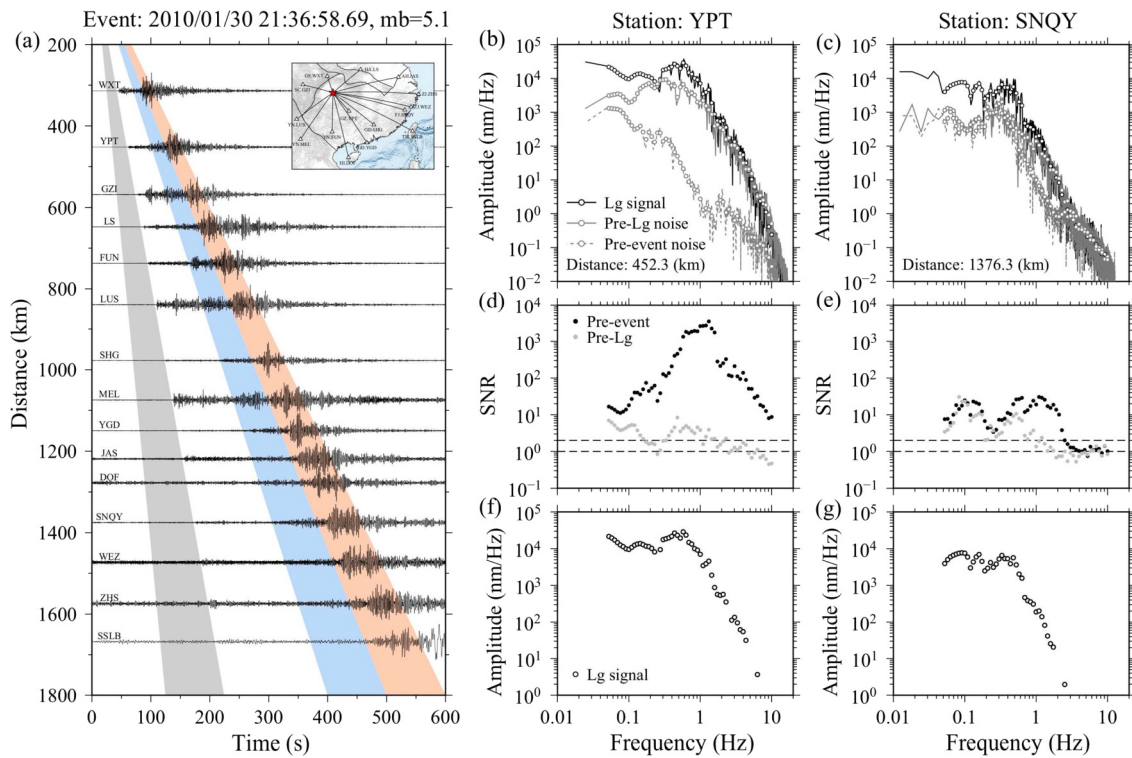
Fig. 2. (a) Selected seismograms from an earthquake occurred on 2010/01/30 in the Sichuan Basin. Normalized vertical-component velocity records filtered between 0.05 and 10.0 Hz are aligned by the origin time and epicentral distances. The colors illustrate the group velocity windows of the Lg-waves (orange), and pre-event (gray) and pre-Lg (light blue) noise windows. The inset map shows the great circle paths from the epicenter (red star) to stations (white triangles). (b-g) The data processing procedure for two sample seismograms recorded by stations YPT and SNQY, including the Fourier spectral amplitude for Lg-wave and noise spectra (b and c), signal-to-noise ratios (d and e), and the Lg signals after corrected by pre-event noise (f and g).

signal and noise, and the noise is stationary and uncorrelated with the signal (Ringdal et al., 1992), we can remove the pre-event noise from the observed spectra and obtain the Lg-wave spectral amplitude (Figs. 2f and 2g).

After the data pre-processing, we obtained single-station amplitudes from the observed Lg-wave spectra, from which two-station spectral ratios can be calculated and the source effects can be eliminated. Combining both the single- and two-station data, a joint inversion system can be established to obtain the attenuation (Zhao et al., 2013; Zhao and Xie, 2016). By including the single- and two- station data, we can ensure the ray coverage and

reduce the trade-off between the source effects and attenuation (Figure S2). The Least Square QR factorization algorithm (Paige and Saunders, 1982) with regularization, damping, and smoothing was employed to solve the joint inversion system and calculate the Q_{Lg} model, the source excitations (Figure S3 and Table S1), and the site responses (Figures S4 and S5) at 58 discrete frequencies. For details of the inversion method refer to Text S1 in the Supplementary Information. After the joint inversion, the root mean square (RMS) of residuals is significantly reduced (Figure S6). The distribution of final residuals tends to be Gaussian with a zero mean and a much smaller standard deviation (Fig. 3). The unresolved residuals may
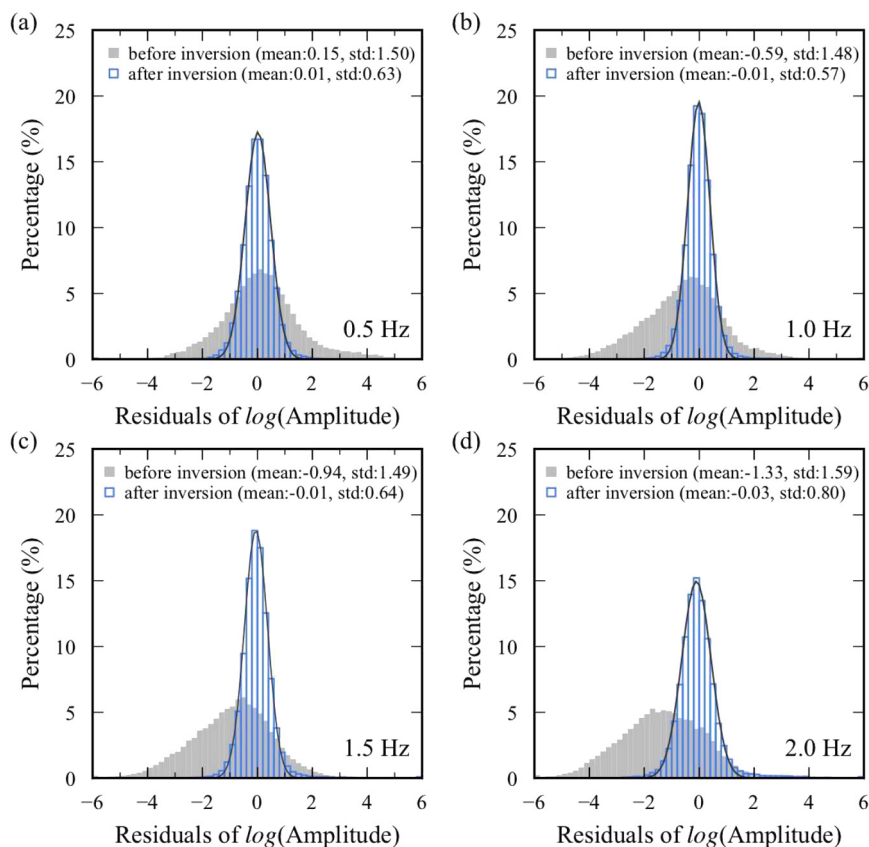
Fig. 3. Distributions of residuals between the observed Lg data and amplitudes predicted by the theoretical attenuation models before (gray) and after (blue) the inversion at selected frequencies, with (a) 0.5, (b) 1.0, (c) 1.5, and (d) 2.0 Hz, respectively. Both the mean and standard deviations are labeled in each panel.

result from the complex source terms and other random effects (e.g., Zhao et al., 2013).

3. Results

3.1. Q_{Lg} maps at individual frequencies

From inversion, the high-resolution broadband crustal attenuation model for the SCB and surrounding areas was obtained at 58 individual frequencies from 0.05 to 10.0 Hz. As examples, Q_{Lg} slices at four selected frequencies, 0.5, 1.0, 1.5, and 2.0 Hz, are shown in Fig. 4a-4d. These attenuation maps reveal the average attenuation for the entire crust depth and include both scattering and intrinsic attenuations. The Q_{Lg} values have similar patterns among different frequency ranges. Strong Lg-wave attenuation with Q_0 (Q_{Lg} at 1.0 Hz) lower than 200 can be found in the western margin of the SCB, such as in the Songpan-Ganzi block and Chuandian block. These regions have intensive crustal deformation and partial melting in the middle and lower crust (Bai et al., 2010; He et al., 2021). The upwelling of the Hainan plume not only caused widely distributed Cenozoic alkaline basalts, but also dramatically increased the temperature of the crust, responding to strong attenuation observed in this region (e.g., Liu et al., 2017). Located at the intersection of double-slab subduction between the Eurasian and Philippine plates, Taiwan Island and its surrounding areas are undergoing intensive tectonic deformations, which is characterized by strong attenuation ($Q_0 < 250$) (e.g., Fan and Zhao, 2021). Compared with these surrounded active regions, the entire SCB is characterized by weak attenuation and higher Q_{Lg} values ($Q_0 > 400$), which is consistent with the high seismic velocity revealed by tomographic results and a stable tectonic environment (Han et al., 2022; Zhou et al., 2012). The NE–SW-trending Q_{Lg} contours in the SCB

almost precisely coincide with the Jiujiang-Shitai buried fault and Jiangshan-Shaoxing-Pingxiang fault, which mark different physical properties among the Jiangnan orogen, the Yangtze Craton, and the Cathaysia block (Shu et al., 2021). The high Q_{Lg} observed in the western part of the Yangtze Craton, i.e., the Sichuan Basin, corresponds to a long-term stable block with a deep cratonic root (e.g., Hearn et al., 2008; Phillips et al., 2005). The relatively low Q_{Lg} values around the southern and eastern parts of the Sichuan Basin may result from compressive deformation due to the eastward movement of the Sichuan Basin relative to the Yangtze Craton, which is also consistent with the conclusion from the velocity imaging (Zhou et al., 2012).

Our crustal Lg attenuation model has higher spatial resolution and covers a wider frequency range, but its major features are comparable with previous results (Chen and Xie, 2017; Hearn et al., 2008; Phillips et al., 2005). For example, Phillips et al. (2005) applied an amplitude ratio tomography technique to obtain the regional Q_{Lg} for central and eastern Asia at 1.0 Hz. Their results show that the Q_{Lg} values of the entire SCB are higher than 350, with the highest Q_0 value (>650) in the Sichuan Basin and the Cathaysia block. Chen and Xie (2017) applied a singular value decomposition method to invert the Q_0 model for the SCB. Their results show that the Cathaysia block is characterized by high Q_0 values of approximately 350~800, where the Wuyishan terrane has the highest value ($Q_0 > 800$) correlating to the Precambrian basement.

3.2. Tomographic Q_{Lg} model appraisal

To assess both the reliability and resolving power of the resulting Q_{Lg} model, we conducted checkerboard tests and calculated uncertainties of Q_{Lg} distributions at all 58 frequencies. Fig. 5 illustrates the path densities, retrieved Q_{Lg} perturbations, and relative
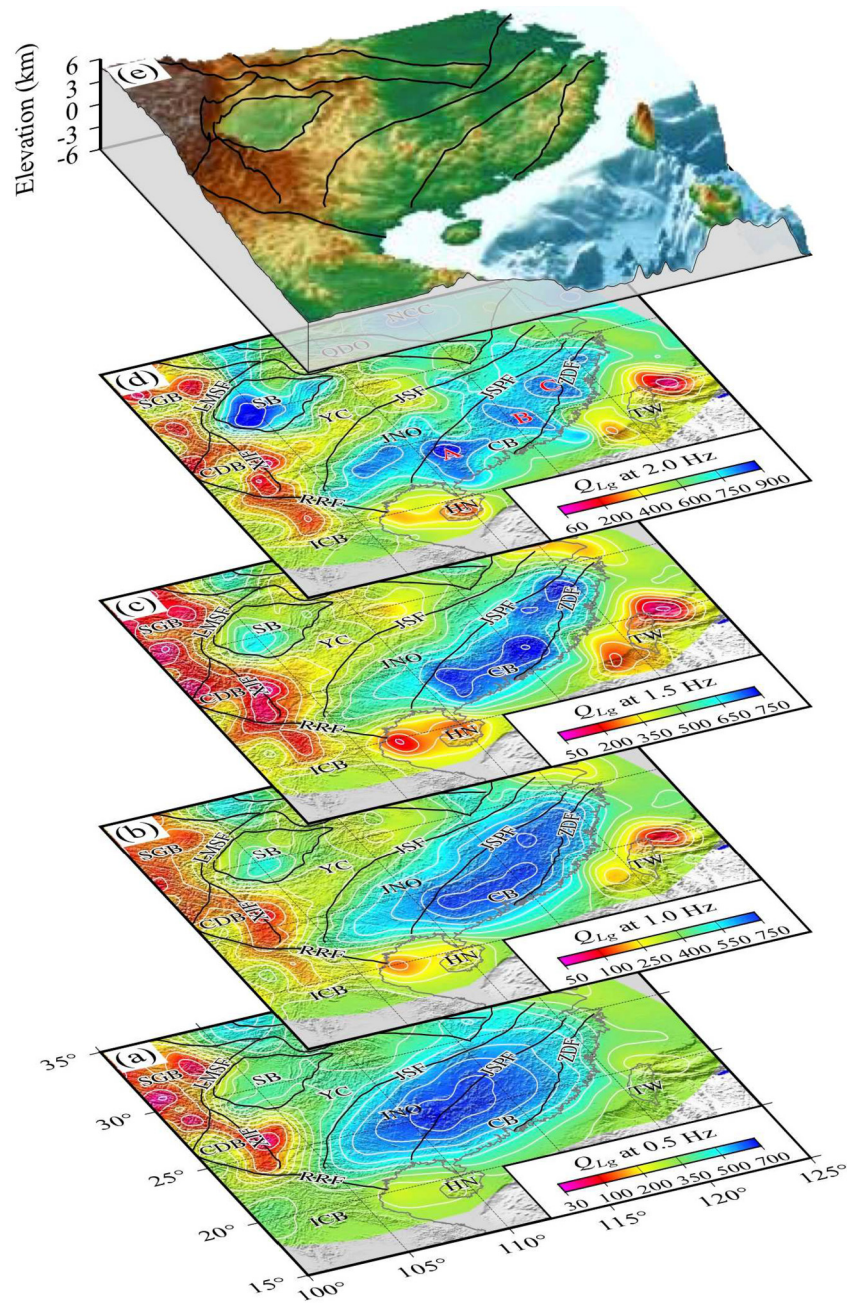
Fig. 4. Q_{Lg} maps at frequencies 0.5 (a), 1.0 (b), 1.5 (c), and 2.0 Hz (d), and a 3D topography map (e) for the SCB overlain by tectonic boundaries and faults (black lines). The red letters A, B, and C in (d) represent the Yunkai, Nanling, and Wuyishan terranes, respectively. Note that different color scales are used for different frequencies to capture the variations. The areas with low seismic ray coverage are cut off.

standard deviations (RSD) at four typical frequencies. In general, the reliability of tomography models depends significantly on the data coverage. The entire SCB is characterized by at least 1000 ray paths in each $1° \times 1°$ grid cell (Fig. 5). In particular, in the Sichuan Basin, the ray density reaches to more than 2000 per grid space. Based on the high-density raypath coverage, we used a checkboard method to evaluate the spatial resolution of our tomography strategy (e.g., Morgan et al., 2002). By creating a checkerboard Q_{Lg} model composed of 7% positive and negative perturbations over a background value, we generated a synthetic dataset based on actual sources, stations and ray paths (e.g., Zhao et al., 2013). Random noises with 5∼10% RMS fluctuations were added to the synthetic data to simulate the real data (e.g., He et al., 2021). Then, the noise-added synthetic data were used in the inversion. By investigating the inverted results (Fig. 5), the spatial resolution

in the SCB can approach to $1° \times 1°$. We also examined the RSD of our tomographic Q_{Lg} model using the bootstrapping technique (Efron, 1983). At a given frequency, 80% of ray paths were randomly selected from the Lg dataset to establish 100 partial bootstrap datasets, from which 100 Q_{Lg} images were obtained. The RSD value between the Q_{Lg} values from partial datasets and the Q_{Lg} value from the complete dataset can be statistically calculated at each location. Complete calculations for all locations in the image, an RSD map can be obtained as shown in Fig. 5. The RSD values lower than 6% across the entire SCB demonstrate the robustness of our tomographic results. Due to less dense raypath coverage, the marginal areas, such as regions surrounding the SCB, are characterized by relatively large RSD values, but they are still lower than 20%.
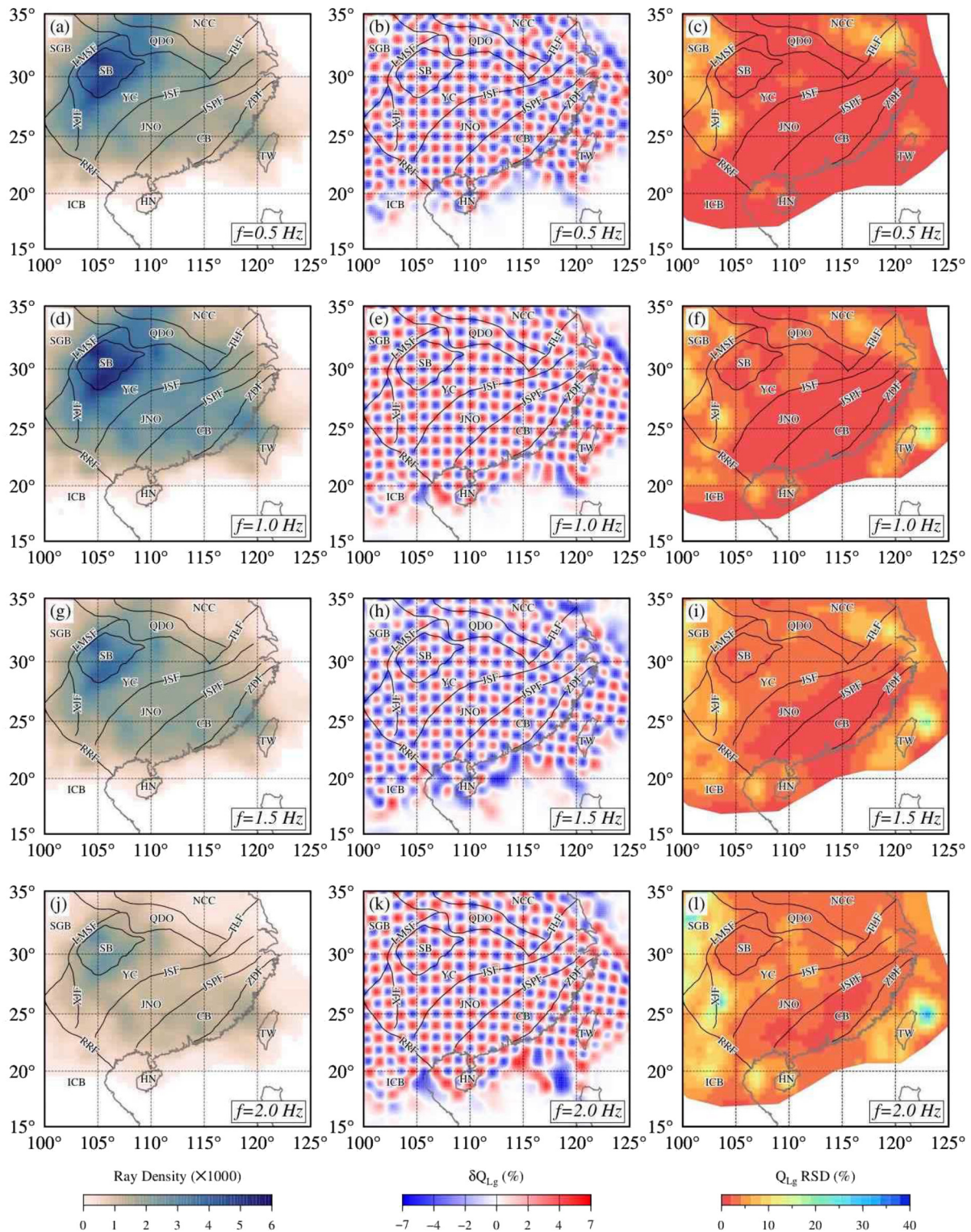
Fig. 5. Raypath densities (left column), resolution analyses (middle column), and RSD values for Q_{Lg} model uncertainty (right column) at frequencies 0.5 (a-c), 1.0 (d-f), 1.5 (g-i), and 2.0 Hz (j-l). Note that the ray path densities include both single- and two-station data.

3.3. Broadband Q_{Lg} images

Even though the Q_{Lg} values have similar large-scale patterns over different frequencies, they show different details at individual frequencies. Therefore, we calculated average Q_{Lg} values within a selected frequency band to better characterize regional attenuations in geological units of different types. Here, we calculated the frequency dependence of mean Q_{Lg} within a given geolog-

ical block, and then investigated variations of mean Q_{Lg} versus frequency relations across different geological blocks (Fig. 6). The mean Q_{Lg} values increase steeply with frequency at above 2.0 Hz. The strong frequency dependence may be resulted from scattering induced attenuation. Between 0.2 and 2.0 Hz, the mean Q_{Lg} values are more robust than at other frequencies in characterizing the regional attenuation variations. Therefore, we calculated the average Q_{Lg} value between 0.2 and 2.0 Hz and used it to
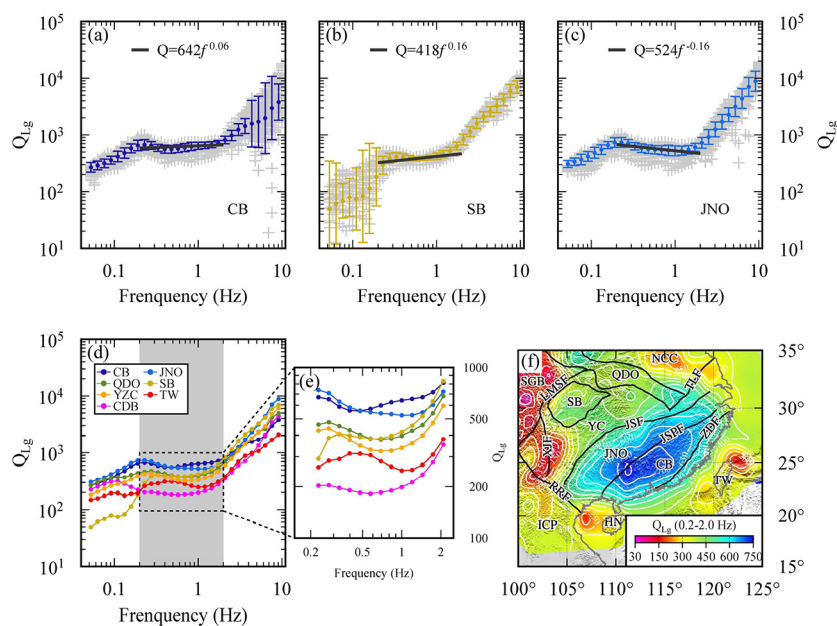
Fig. 6. Comparison between frequency-dependent Q_{Lg} models at different subregions. Q_{Lg} versus frequency for selected blocks, with (a) the Cathaysia block, (b) the Sichuan Basin and (c) the Jiangnan orogen. The directly inverted Q_{Lg} values at a given frequency are shown as gray crosses, along with their average values and logarithmic standard deviations (error bars). By fitting the Q_{Lg} values between 0.2 and 2.0 Hz, power-law Q_{Lg} models can be obtained and shown as black lines. (d) Frequency-dependent Q_{Lg} curves for all geoblocks in and around the SCB, in which the gray shaded area is enlarged and shown as (e). (f) Map showing the Q_{Lg} distribution averaged between 0.2 and 2.0 Hz.

Table 1
Lg attenuation, crust and heat flow parameters for individual geological blocks.

Geological block		Crust model[a]		Heat flow model[b]	Lg attenuation		
Name	Abbreviation	Crust thickness (km)	Sediment thickness (km)	Heat flow (mW/m³)	Q_0 (1.0 Hz Q)	Q (0.2~2.0 Hz)	η (0.2~2.0 Hz)
Cathaysia block	CB	30.3±1.5	0.03±0.07	70.2±11.6	642 (556-741)	607±74	0.06±0.03
Chuandian block	CDB	42.1±2.6	0.41±0.64	74.3±17.0	199 (155-254)	214±58	0.05±0.04
Jiangnan orogen	JNO	32.9±2.9	0.44±1.13	65.6±12.0	524 (429-640)	567±75	−0.16±0.04
Qinling-Dabie orogen	QDO	38.3±6.0	0.25±0.66	58.8±12.9	397 (317-499)	427±69	−0.05±0.05
Sichuan Basin	SB	41.4±2.6	7.12±1.30	53.7±8.4	418 (366-478)	424±38	0.16±0.05
Taiwan Island	TW	31.0±9.0	0.58±0.26	118.8±100.9	274 (221-338)	332±15	−0.12±0.06
Yangtze Craton	YZC	37.9±4.8	3.47±2.84	58.1±11.6	338 (252-454)	396±98	−0.10±0.05

[a] From CRUST 1.0 (Laske et al., 2013).
[b] From Mainland China heat flow (Jiang et al., 2019).

compare crust attenuation properties among geological blocks of different types (Fig. 6e). The lateral variations in the average Q_{Lg} map illustrate that the Q_{Lg} patterns are generally similar to those at single frequencies and correlate well with regional tectonics. Since the Q_{Lg} values were inverted independently at individual frequencies, we further used the power law model $Q(f) = Q_0 f^\eta$ to fit the $Q(f)$ between 0.2 and 2.0 Hz and estimate the Q_0 and the frequency-dependency parameter η. The η ranges from −0.116 to 0.159. In summary, the estimated crustal Q_0, average Q_{Lg} value, and η can be used to characterize the individual geoblocks, similar to commonly used parameters such as the average crustal thickness, sedimentary thickness, and surface heat flow (Table 1).

Using the frequency-dependent Q_{Lg} cross-sections, we can explore crustal characteristics on both the large-scale structural variations and small-scale heterogeneities among different blocks (Fig. 7). If the scattering attenuation dominates the Lg-wave attenuation, the frequency absorbing band provides information regarding the scale of heterogeneities, that is the higher frequency corresponds with the smaller scatters (e.g., Sato et al., 2012; Wu et al., 2000). Thus, the Q_{Lg} within a certain frequency band may provide information regarding the corresponding scales of heterogeneities. The frequency profile crossing the Longmenshan fault shows a prominent boundary between the Tibetan Plateau and

the SCB, which is characterized by a steep Q_{Lg} gradient turning from the low-Q_{Lg} Tibetan Plateau to the high-Q_{Lg} SCB sharply (Figs. 6f, 7a, and 7b). The steep gradient may reflect a strong interaction between the eastern margin of the Tibetan Plateau and the Yangtze Craton. Strong attenuation (low Q_{Lg}) between 0.05 and 3.0 Hz beneath the western margin of the Yangtze Craton can be attributed to extensive partial melting and/or lower crustal flow due to strong deformation by southeast extrusion outward from the Tibetan Plateau (Figs. 7c and 7d) (e.g., Bai et al., 2010; Tapponnier and Molnar, 1976). As the largest strike-slip fault in eastern China, the Tanlu fault cuts through the lithosphere, acting as a major channel for asthenospheric upwelling, which is characterized by strong attenuation between 0.5 and 1.5 Hz (Fig. 7a) (e.g., Chen et al., 2006). The SCB is characterized by weak crustal Lg attenuation and relatively small lateral variations among different sub-blocks, correlating with other geophysical observations (e.g., Han et al., 2022; Zhang et al., 2015) (Fig. 7). However, relatively low-Q_{Lg} between 0.5 and 5.0 Hz can be observed beneath the Yangtze craton, whereas the Cathaysia block is characterized by high-Q_{Lg} within this frequency band (Figs. 7b and 7c). Note that local attenuation variations can be observed between the Jiangnan orogen and the Cathaysia block within the SCB (Figs. 7c and 7d). Due to the thick sedimentary layers, the Sichuan Basin is featured by low Q_{Lg} at frequencies less than 0.2 Hz (Fig. 7c) (e.g., He et al., 2021; Mitchell
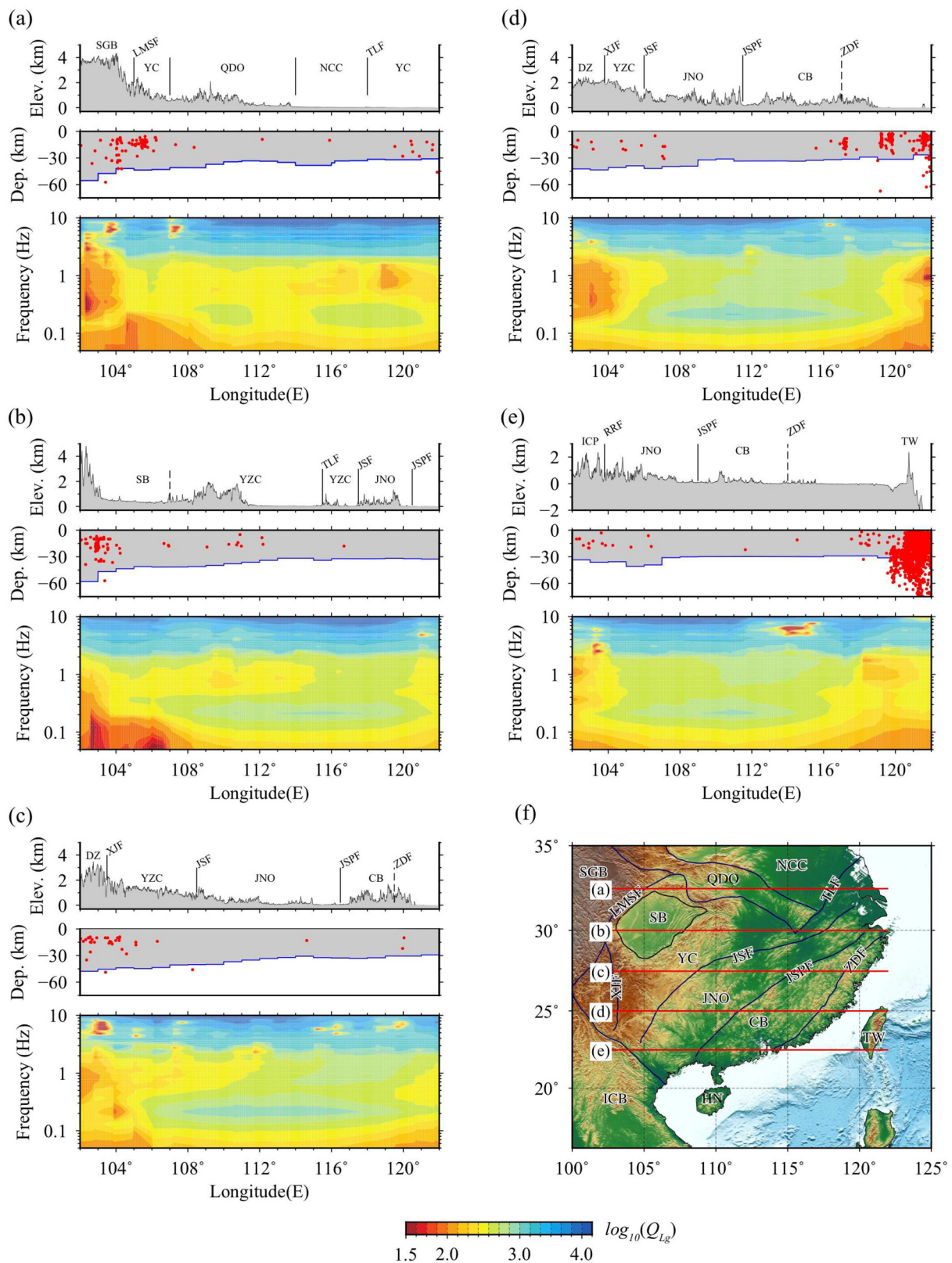
Fig. 7. Cross-sections showing surface topography (upper), crust and uppermost mantle structures and the seismicity (middle), and Q_{Lg} versus frequency profiles for latitudes (a) 32.5°N, (b) 30°N, (c) 27.5°N, (d) 25°N, and (e) 22.5°N. Their locations are marked with red lines in the regional map (f). The map is also overlain by geological blocks, major faults, Moho depth (blue) from CRUST 1.0 (Laske et al., 2013), and earthquakes (red dot) with magnitudes higher than 2.5 and occurred between 2000 and 2018. The abbreviations are the same as those in Fig. 1.

and Hwang, 1987). Small-scale strong attenuation areas at high frequencies between 5.0 and 10.0 Hz often exist near some fault belts, such as the Jianshan-Shaoxing-Pingxiang fault (Fig. 7c) and

the Zhenghe-Dapu fault (Fig. 7e), which are probably related to the scattering attenuation caused by small-scale heterogeneities (e.g., Wu et al., 2000). Low frequency high Q_{Lg} values are broadly existed

beneath the SCB, indicating some large-scale crystalline basement in the lower crust.

4. Discussion

4.1. Origin of high Q_{Lg} in the Cathaysia block

Crustal Q_{Lg} depends on physical, chemical, lithological and mineralogical properties of the crust, and hence closely relates to factors including the rock age, rheology strength, thermal status, degree of heterogeneity, and crust thickness (e.g., Fan and Lay, 2002; Zhang and Lay, 1995). Therefore, the high Q_{Lg} in the Cathaysia block may reflect crustal features, such as ancient materials, low temperatures, material homogeneity, stability, thick crust and/or high rheological strength.

The surface heat flow in the Cathaysia Block was observed to be approximately 69.4 ± 11.0 mW/m^2, which is higher than the average global continental heat flow value of 65 ± 1.6 mW/m^2 (e.g., Jiang et al., 2019). This is obviously inconsistent with the high Q_{Lg} value in this region. Zhang et al. (2018) suggested that the high temperatures in the shallow crust result from the heat produced by the decay of the radioactive elements in the granite and that the overall crustal temperature is low. By using numerical modeling, Sun et al. (2013) obtained a 3D thermal structure model for Mainland China and adjacent regions and suggested that the temperature is approximately $600\,^{\circ}$C at the Moho of the SCB, indicating a typical thermal state for the Precambrian craton compared with high temperatures ($>800\,^{\circ}$C) beneath orogens or plate boundary zones. However, the mantle lithosphere beneath the Cathaysia block shows relatively high temperatures at a depth of 60 km (Sun et al., 2013). Therefore, it is difficult to say the high Q_{Lg} in the Cathaysia block is due to low temperatures.

To investigate how the crustal thickness affects the Q_{Lg}, we calculated average Q_{Lg} values and crustal thicknesses for individual geological blocks. Because the low-frequency Lg-waves are more sensitive to the crustal thickness (e.g., Zhang and Lay, 1995), the Q_{Lg} values between 0.2 and 1.0 Hz were adopted to investigate the relationship between the attenuation and crustal thickness (Fig. 8) (Zhao et al., 2013; Zhao and Xie, 2016). In general, the theoretical prediction suggests that the thicker the crust is, the more Lg-wave overtones can be transmitted and hence the Lg-wave can be more efficiently propagated (Zhang and Lay, 1995). Therefore, thicker crust results in higher Q_{Lg} value. As indicated by green colored area in Fig. 8, observations from East Asia confirm this relation. However, when an area is tectonically very active or very stable, such a relationship may be affected, as can be seen the Tibetan Plateau has very low Q_{Lg} and very thick crust while some blocks in the SCB have very high Q_{Lg} but relatively thin crust (Fig. 8). This indicates that, compared to the crustal thickness, tectonic activity is a more dominant factor controlling the Q_{Lg} value (Zhao et al., 2013; Zhao and Xie, 2016). Nowadays, the Cathaysia block is a stable and rigid block without any obvious internal velocity gradient and deformation based on GPS data (Wang and Shen, 2020). Under the stable tectonic environment, fluids in the faults and cracks are lost or absorbed due to migration to the surface or retrograde metamorphism, which results in the closure of the faults and further increases the Q values (e.g., Mitchell, 1995). Also, within a stable block, there is less tectonic activated hydrothermal release which would increase the Q values (e.g., Mitchell, 1995). On the other hand, the crustal thinning and reworking may increase the strength of the Cathaysia block and lead to high Q_{Lg} values (Deng and Tesauro, 2016; Hearn et al., 2008). The Paleo-pacific subduction caused an extensional environment in the Cathaysia during the Mesozoic, and hence asthenosphere upwelling occurred, inducing partial melting of the Proterozoic basement and underplating of mantle-derived magmas, which strongly changed the physical
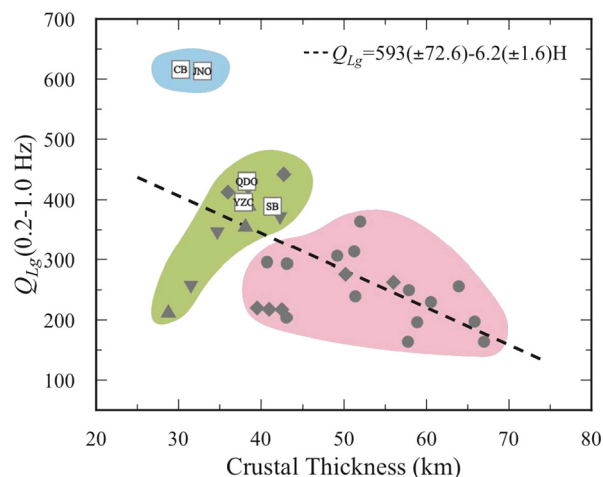
Fig. 8. The average Q_{Lg} values between 0.2 and 1.0 Hz versus average crust thickness for selected geological blocks. The symbols are listed in Table S2. The black dashed line represents linear regression between Q_{Lg} and crust thickness. Note that the geological blocks in green area obey the theoretical positive relationship between Q_{Lg} and crustal thickness, whereas others strongly break up the theoretical prediction, where the CB and JNO in the blue area are characterized by extremely high strength, and the geological blocks in the pink region are tectonically active.

property and composition of the lower crust (e.g., Chen et al., 2022a; Wang et al., 2013). After cooling and solidification, these Mesozoic intrusive rocks and mixed mantle peridotites crystallized as the high-strength basement in the crust, which significantly reduce the crustal heterogeneity, increase the wave propagation efficiency, and therefore increase the Q_{Lg} for the Cathaysia block (e.g., Hearn et al., 2008). The large scale high-Q_{Lg} region between 0.1 and 0.5 Hz beneath the SCB may correspond with these reworked crystalline basement (Fig. 7). Therefore, the high Q_{Lg} values in the Cathaysia block can be attributed to its extremely stable environment and rigid crust, which are also supported by other observations, such as relatively high P- and S-wave velocities (e.g., Han et al., 2022; Zhang et al., 2013), very high resistivity (e.g., Yin et al., 2021; Zhang et al., 2020), and elevated strength (Deng and Tesauro, 2016). Exceptionally, the Sichuan basin is a stable Archean craton with a thick lithospheric root but, compared to other similar structure, it has a relatively lower Q_{Lg} value at lower frequencies (Fig. 7b and 8), which is likely due to the very thick sedimentary layers in the basin which strongly attenuated the Lg-wave propagation (e.g., He et al., 2021; Mitchell and Hwang, 1987).

Even though the crust was strongly reworked and much of the Precambrian geological records were obscured after multiple stages of Phanerozoic tectonic evolution, the isotope ages for detrital and xenolith zircons in sediments and igneous rocks reveal that the unexposed Paleoproterozoic or the Archean basement is likely buried beneath the Cathaysia block (e.g., Yu et al., 2009; Zhang and Zheng, 2013; Zheng et al., 2011). These potential unexposed ancient materials may also contribute to the high-Q_{Lg} for the Cathaysia block (e.g., Mitchell, 1995). Therefore, the ancient basement in the deep crust and the remelted crystallized rocks in the Mesozoic may combine together to create a rigid and stable crust that features a high Q_{Lg} Cathaysia block.

4.2. Ancient continental relics within the crust of the SCB

It is widely accepted that the Yangtze Craton is consisted of an Archean-Paleoproterozoic crystalline basement overlain by shallow crust partially reworked in the Phanerozoic (e.g., Zhao and Cawood, 2012; Zheng et al., 2006). The Precambrian basement rocks are sparsely exposed in the Cathaysia block and were therefore considered a Paleozoic fold belt rather than an old block (e.g.,
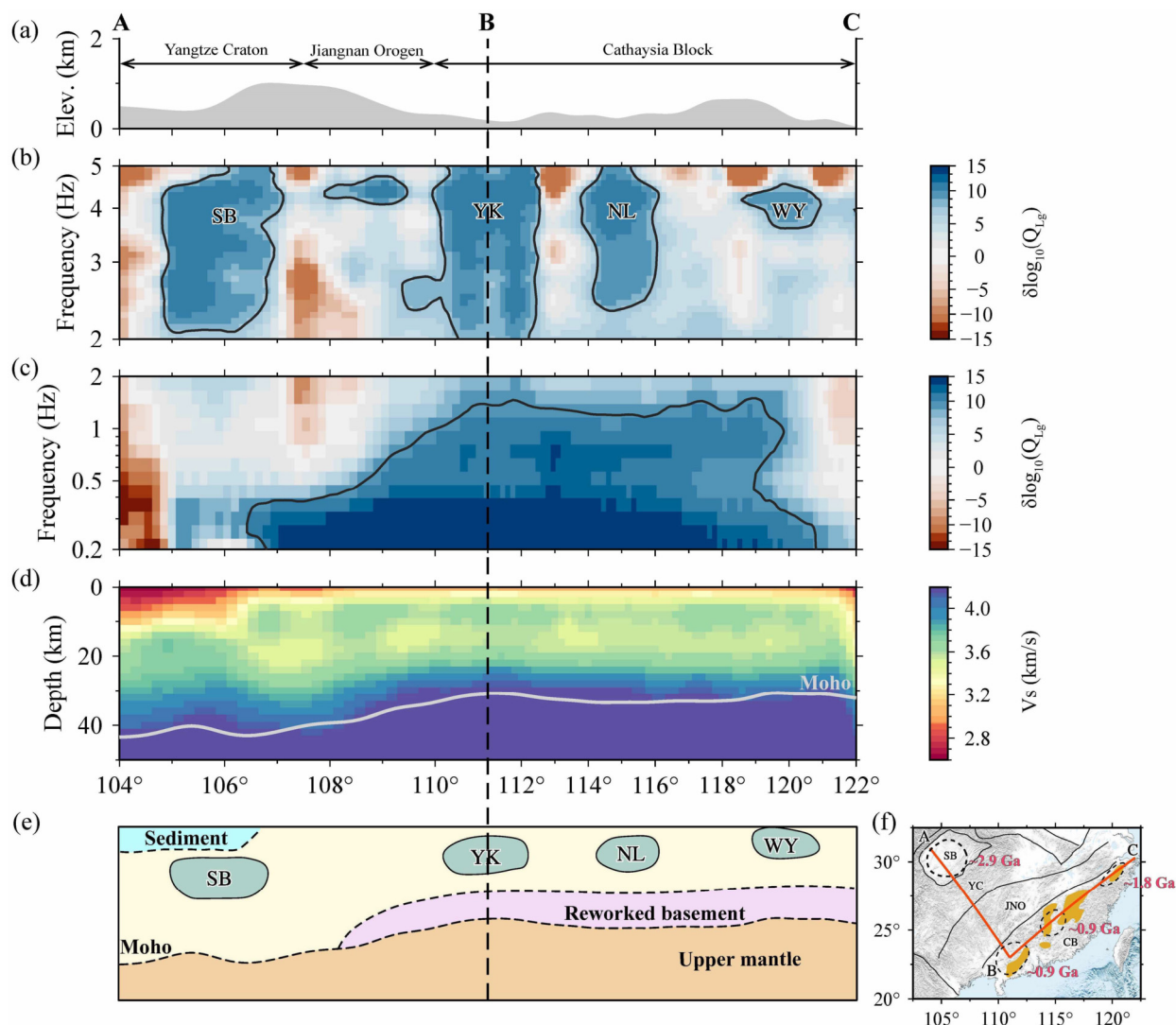
Fig. 9. Combined cross-sections along four potential ancient continental relicts in the SCB, including surface topography (a), percentage Q_{Lg} perturbations versus frequency between 2.0 and 5.0 Hz (b), and between 0.2 and 2.0 Hz (c), S-wave velocity (Han et al., 2022) (d), a schematic interpretation of the relation between the attenuation and current day crust structure (e), and surface locations of the profile (red lines in (f)). The black contours in (c) and (d) denote the 7% and 9% Q_{Lg} perturbations against a background Q_{Lg} at individual frequencies, respectively. The ancient continental relicts beneath the SCB inferred from the attenuation model are indicated by green shaded areas in (e), and also circled by dashed lines in (f), with their ages labeled. The orange-colored areas in (f) represent the ancient continental fragments suggested by Shu (2006). The abbreviations are NL, Nanling; WY, Wuyishan; and YK, Yunkai. Other abbreviations are the same as those in Fig. 1.

Ma, 2006). Recently, by using the dating of detrital and xenocrystic zircons, geochronological studies revealed the existence of unexposed Archean-Paleoproterozoic crust underneath the Cathaysia block (e.g., Xu et al., 2005; Yu et al., 2010). The high Q_{Lg} values we observed in the Cathaysia crust also imply that Archean-Paleoproterozoic continental fragments exist in the current crust.

Based on four high-Q_{Lg} zones in the SCB, the potential locations of ancient continental relicts can be determined, with one beneath the Sichuan Basin and the other three in the Cathaysia block (Figs. 4c and 4d). These four zones are mainly reflected in the high frequency (>1.0 Hz) attenuation maps (Figs. 4 and 9). Dense ray coverage of Lg-waves permits us to obtain a high-resolution tomographic model to better constrain horizontal locations of these ancient continental relicts. The Lg wave samples the entire crust. Even though it does not have the depth resolution in the crust, combining with velocity tomographic models, which has relatively higher vertical resolution within the crust, we can roughly estimate the depth of these ancient continental relicts (e.g., Han et al., 2022; Li et al., 2022; Wu et al., 2000). Several zones with S-wave velocity greater than 3.6 km/s can be observed at depths between

5 and 15 km in the velocity profile, which roughly correspond to the extremely high Q_{Lg} regions between 2.0 and 5.0 Hz in the Cathaysia block (Fig. 9b and d). Relatively low Q_{Lg} region around 2.0 Hz may correspond with these low S-wave velocity zones in the middle crust (~15-20 km). These low-velocity zones may be caused by the multi-phase magmatic events (Li et al., 2022) or the formation of compositional and structural layering in the tectonic quiescence period during the late Neoproterozoic to the early Phanerozoic (Chen et al., 2022b). Therefore, the ancient continental relicts likely located in the upper crust of the Cathaysia block. In contrast, the high Q_{Lg} region observed at relatively low frequency between 0.2 and 1.0 Hz may correspond to the homogeneous basement in the crust, which is consistent with high S-wave velocities of approximately 4.0~4.2 km/s in the lower crust. The reworked and crystallized lower crust may contribute to the high Q_{Lg} in the lower frequency in the Cathaysia block, which is consistent with the strengthening seismic reflection in the lower crust and a felsic crustal composition with Vp/Vs of about 1.74 in this region (Chen et al., 2022a; Hearn et al., 2008; Li et al., 2022; Zhang et al., 2013). However, the reworking degree may vary based on

the observed laterally varying Vp/Vs ratios across the Cathaysia block (Chen et al., 2022a; Li et al., 2022). Compared with the coastal terrane characterized by intensive magmatic underplating and voluminous mantle influx, the interior terrane of the Cathaysia block shows relatively weak magmatic modification and is considered mainly as a Neoproterozoic amalgamation terrane (Dong et al., 2020). Therefore, based on the extremely weak attenuation there, the ancient continental relics are mainly concentrated in the inland area of the Cathaysia block (Shu, 2006) (Fig. 4c, 4d, and 9f). Thus, the inland part of the Cathaysia block can be composed of highly evolved Precambrian continental materials in the upper crust, and reworked crystalline basement in the middle and lower crust (Fig. 9e).

The Sichuan Basin is covered by a roughly 10 km thick sedimentary layer (Laske et al., 2013), which can obscure early geological records from the Proterozoic basement. However, Archean and Paleoproterozoic basement rocks are exposed around the Sichuan Basin (e.g., Wang et al., 2018; Zhao and Cawood, 2012). Therefore, the ancient crystalline basement with ages 2.6 Ga or older beneath the Sichuan Basin is likely unexposed (e.g., Wang et al., 2018; Zheng et al., 2006). The ancient continental nucleus in the Sichuan Basin, featuring a low rate of seismicity, low strain rate ($<2.0 \times 10^{-9}$/year), and low heat flow ($\sim$53 mW/m^2), is a rigid and cold tectonic block without obvious deformation (e.g., Jiang et al., 2019; Wang and Shen, 2020). As a long-term stable craton, the Sichuan Basin is characterized by high velocity (Han et al., 2022; Zhou et al., 2012), weak attenuation (e.g., Phillips et al., 2005), and high resistivity ($>$1000 $\Omega \cdot$m) (e.g., Zhang et al., 2015). Deng et al. (2021) observed extremely weak teleseismic body-wave attenuation with $\Delta t_p^* < -0.1$ for the lithosphere-asthenosphere system in the Sichuan Basin. Hearn et al. (2008) used seismic amplitude tomography to estimate the weak crustal attenuation to correspond with high Q_0 greater than 1000 in this region. Our Lg attenuation model shows extremely weak attenuation with over 7% positive Q_{Lg} perturbation based on the background Q_{Lg} values on the logarithmic scale between 2.0 and 5.0 Hz, which may better characterize the Archean continental nucleus beneath the Sichuan Basin (Fig. 7b). The Sichuan Basin is dominated by intermediate to mafic rocks and thick cratonic mantle root, and is tectonically stable (e.g., Chen et al., 2022a). Therefore, it is similar to the Ordos basin and may also be formed by thick trapped oceanic plateaus (Kusky and Mooney, 2015).

The Wuyishan terrane in the Cathaysia block is considered an ancient continental nucleus due to the oldest Precambrian basement rocks ($\sim$1.8 Ga) exposed in the northern Wuyishan terrane (e.g., Shu et al., 2021). Yu et al. (2009) suggested that the Wuyishan terrane is a long-lived remnant of the old craton that has survived for at least one billion years given the abundant Archean inherited zircons (2.5$\sim$2.7 Ga) in the Paleoproterozoic rocks. A deep seismic reflection profile across the Wuyishan terrane reveals the existence of a high-strain Proterozoic basement based on abundant reflections in the crust (Dong et al., 2020). Chen and Xie (2017) obtained a weak attenuation region with Q_0 values higher than 800 in the Wuyishan terrane. From the broadband Lg attenuation obtained in this study, the Wuyishan terrane is also characterized by weak attenuation with over 7% positive Q_{Lg} perturbation on the logarithmic scale, which is similar to that in the Sichuan Basin and corresponds to the Paleoproterozoic or even Archean continental fragments in the crust.

However, the surface Precambrian rocks in the Nanling and Yunkai terranes consist only of Neoproterozoic igneous rocks ($\sim$0.9 Ga) without Archean to Paleoproterozoic basement outcrops (e.g., Yu et al., 2010; Zhao and Cawood, 2012). Unexposed Archean basement rocks likely underlie these two terranes from the detrital and xenocrystic zircons (e.g., Zhang and Zheng, 2013). The zircon xenoliths from the Mesozoic basalts in the Yunkai area contain numerous ancient crustal components with several stages of reworking, implying the existence of a highly evolved unexposed Archean-Paleoproterozoic basement (e.g., Li et al., 2018). In the Nanling range, Xu et al. (2005) reported the presence of Archean zircons in Mesoproterozoic gneiss and Devonian sedimentary rocks, and suggested that the central parts of the Cathaysia block contain Archean microcontinental fragments. The age distribution and elemental geochemical features of the zircons are similar to those obtained from the nearby sedimentary rocks, which conversely better constrain the source of the zircons (Li et al., 2018; Xu et al., 2005). However, these zircons may experience multiple cycles and travel long-distance from unknown blocks that were once contiguous to the Cathaysia block, because the Archean zircons are usually oval with complex textures (Li et al., 2014). Thus, the ancient continental fragments in the Yunkai and Nanling terranes are of at least early Neoproterozoic age according to the surface exposed rocks (Shu et al., 2021). The high resistivity ($>$2000 $\Omega \cdot$m) in the Nanling and Yunkai terranes from the surface to depths greater than 150 km may result from a dry or low-water-content environment, which matches the rheological characteristics of the cratonic lithosphere (Yin et al., 2021; Zhang et al., 2020). Similar to both the Sichuan Basin and the Wuyishan terrane, these regions are characterized by extremely weak attenuation with 7% positive Q_{Lg} perturbation on the logarithmic scale and reveal the unexposed Precambrian continental relics in the current crust (Fig. 9b).

Lithologic, chronological, and geochemical data from the Precambrian basement suggest that the Cathaysia block might have been assembled by multiple blocks or arcs from different tectonic domains in an accretionary subduction environment rather than existing as a unified block during the early Neoproterozoic (Wang et al., 2014; Yao et al., 2017; Yu et al., 2010). The three extremely high-Q_{Lg} regions provide the approximate locations for the Precambrian sub-blocks making the Cathaysia block. Considering the age and composition of the Precambrian outcrops, Shu et al. (2021) suggested that the Cathaysia block was likely assembled by western expansion from the Wuyishan to the Nanling and Yunkai terranes in the Neoproterozoic. Yao et al. (2019) suggested that the Jiangnan orogen is an accretionary orogenic belt, which consists of three distinct tectonostratigraphic arc-trench-basin assemblages during the Neoproterozoic, including the northeast, the central, and the southwest domains. Corresponding with three distinct tectonic domains in the Jiangnan orogeny, the three sub-blocks in the Cathaysia block may accrete and collide along the margin of the Yangtze Craton under a series of convergent plate margin arc systems during the Neoproterozoic. The accretion and subduction environment in the Neoproterozoic period may respond to an external position for the SCB in Rodinia (Cawood et al., 2020, 2017).

5. Conclusions

We developed a broadband Lg-wave attenuation model for the SCB and surrounding regions between 0.05 and 10.0 Hz. The resolution is approximately 1°. The Q_{Lg} distributions correlate well with regional tectonics. The entire SCB is characterized by weak attenuation, which implies a tectonically stable environment. In contrast, strong Lg-wave attenuations were observed in certain surrounding areas, such as the Songpan-Ganzi block, Chuandian block and Taiwan, where strong tectonic activities and partial melting may have occurred. Four areas with extremely weak attenuation likely relate to an Archean nucleus of the Yangtze Craton beneath the Sichuan Basin, and three Precambrian continental fragments within the crust of the Cathaysia block. Based on surface lithological evidence, these Precambrian continental relics have different ages and hence suggest that the SCB was located along the external margin of the Rodinia supercontinent.

CRediT authorship contribution statement

Lin Shen: Conceptualization, Formal analysis, Investigation, Methodology, Software, Visualization, Writing – original draft, Writing – review & editing. **Lian-Feng Zhao:** Conceptualization, Data curation, Funding acquisition, Methodology, Project administration, Resources, Software, Supervision, Validation, Writing – review & editing. **Xiao-Bi Xie:** Methodology, Supervision, Writing – review & editing. **Geng Yang:** Methodology, Software, Writing – review & editing. **Zhen-Xing Yao:** Funding acquisition, Supervision.

Declaration of competing interest

The authors declare that they have no known competing financial interests or personal relationships that could have appeared to influence the work reported in this paper.

Data availability

The waveforms used in this study were collected from the National Earthquake Data Center (NEDC) at https://data.earthquake.cn/yhsj/info/2016/5596.html (in Chinese, last accessed August 2022) and the Incorporated Research Institutions for Seismology Data Management Center (IRIS-DMC) at https://ds.iris.edu/wilber3/find_event (last accessed August 2022). Researchers can register for an account to apply for the NEDC data. Both the Lg and noise waveforms collected from the NEDC can be accessed at the World Data Centre for Geophysics, Beijing (WDCGB) at https://doi.org/10.12197/2022GA026 (last accessed August 2022). The single- and two-station Lg amplitude data used in this study and the resulted broadband Lg-wave attenuation model in the SCB can be accessed at the WDCGB at https://doi.org/10.12197/2022GA022 (last accessed August 2022). Some figures were generated using Generic Mapping Tools (GMT; https://www.generic-mapping-tools.org/).

Acknowledgements

Appendix A. Supplementary material

Supplementary material related to this article can be found online at https://doi.org/10.1016/j.epsl.2023.118144.

References

Bai, D.H., Unsworth, M.J., Meju, M.A., Ma, X.B., Teng, J.W., Kong, X.R., Sun, Y., Sun, J., Wang, L.F., Jiang, C.S., Zhao, C.P., Xiao, P.F., Liu, M., 2010. Crustal deformation of the eastern Tibetan plateau revealed by magnetotelluric imaging. Nat. Geosci. 3, 358–362.

Biggs, J., Ayele, A., Fischer, T.P., Fontijn, K., Hutchison, W., Kazimoto, E., Whaler, K., Wright, T.J., 2021. Volcanic activity and hazard in the East African Rift Zone. Nat. Commun. 12, 6881.

Brune, S., Kolawole, F., Olive, J.-A., Stamps, D.S., Buch, W.R., Buiter, S.J.H., 2022. Geodynamics of continental rift initiation and evolution. Nat. Rev. Earth Environ.

Cawood, P.A., Wang, W., Zhao, T., Xu, Y., Mulder, J.A., Pisarevsky, S.A., Zhang, L., Gan, C., He, H., Liu, H., Qi, L., Wang, Y., Yao, J., Zhao, G., Zhou, M.-F., Zi, J.-W., 2020. Deconstructing South China and consequences for reconstructing Nuna and Rodinia. Earth-Sci. Rev. 204, 103169.

Cawood, P.A., Zhao, G., Yao, J., Wang, W., Xu, Y., Wang, Y., 2017. Reconstructing South China in Phanerozoic and Precambrian supercontinents. Earth-Sci. Rev. 186, 173–194.

Chen, C., Lü, Q., Chen, L., Shi, D., Yan, J., Ai, Y., 2022a. Crustal thickness and composition in the South China Block: constraints from earthquake receiver function. Sci. China Earth Sci.

Chen, J., Pan, L., Li, Z., Chen, X., 2022b. Continental reworking in the eastern South China Block and its adjacent areas revealed by F-J multimodal ambient noise tomography. J. Geophys. Res. 127.

Chen, L., Zheng, T., Xu, W., 2006. A thinned lithospheric image of the Tanlu Fault Zone, eastern China: constructed from wave equation based receiver function migration. J. Geophys. Res. 111, B09312.

Chen, Y.L., Xie, J.K., 2017. Resolution, uncertainty and data predictability of tomographic Lg attenuation models-application to Southeastern China. Geophys. J. Int. 210, 166–183.

Deng, Y., Byrnes, J.S., Bezada, M., 2021. New insights into the heterogeneity of the lithosphere-asthenosphere system beneath South China from teleseismic body-wave attenuation. Geophys. Res. Lett. 48, e2020GL091654.

Deng, Y., Tesauro, M., 2016. Lithospheric strength variations in Mainland China: tectonic implications. Tectonics 35, 2313–2333.

Dong, S., Li, J., Cawood, P.A., Gao, R., Zhang, Y., Xin, Y., 2020. Mantle influx compensates crustal thinning beneath the Cathaysia Block, South China: evidence from SINOPROBE reflection profiling. Earth Planet. Sci. Lett. 544, 116360.

Efron, B., 1983. Estimating the error rate of a prediction rule: improvement on cross-validation. J. Am. Stat. Assoc. 78, 316–331.

Fan, G., Lay, T., 2002. Characteristics of Lg attenuation in the Tibetan Plateau. J. Geophys. Res. 107 (B10), 2256.

Fan, J., Zhao, D., 2021. P-wave tomography and azimuthal anisotropy of the Manila-Taiwan-Southern Ryukyu region. Tectonics 40, e2020TC006262.

Han, S., Zhang, H., Xin, H., Shen, W., Yao, H., 2022. USTClitho2.0: updated unified seismic tomography models for continental China lithosphere from joint inversion of body-wave arrival times and surface-wave dispersion data. Seismol. Res. Lett. 93, 201–215.

He, X., Zhao, L., Xie, X., Tian, X., Yao, Z., 2021. Weak crust in southeast Tibetan Plateau revealed by Lg-wave attenuation tomography: implications for crustal material escape. J. Geophys. Res. e2020JB020748.

Hearn, T.M., Wang, S., Pei, S., Xu, Z., Ni, J.F., Yu, Y., 2008. Seismic amplitude tomography for crustal attenuation beneath China. Geophys. J. Int. 174, 223–234.

Jiang, G.Z., Hu, S.B., Shi, Y.Z., Zhang, C., Wang, Z.T., Hu, D., 2019. Terrestrial heat flow of continental China: updated dataset and tectonic implications. Tectonophysics 753, 36–48.

Kampfmann, W., Berckhemer, H., 1985. High temperature experiments on the elastic and anelastic behaviour of magmatic rocks. Phys. Earth Planet. Inter. 40, 223–247.

Kennett, B.L.N., 1986. Lg-waves and structural boundaries. Bull. Seismol. Soc. Am. 76, 1133–1141.

Knopoff, L., Schwab, F., Kauselt, E., 1973. Interpretation of Lg. Geophys. J. Int., 389–404.

Kusky, T., Mooney, W., 2015. Is the Ordos Basin floored by a trapped oceanic plateau? Earth Planet. Sci. Lett. 429, 197–204.

Kusky, T., Wang, L., 2022. Growth of continental crust in intra-oceanic and continental-margin arc systems: analogs for Archean systems. Sci. China Earth Sci. 65, 1615–1645.

Laske, G., Masters, G., Ma, Z., Pasyanos, M., 2013. Update on CRUST1.0 - A 1-degree global model of Earth's crust. In: EGU General Assembly Conference.

Lee, C.-T.A., Luffi, P., Chin, E.J., 2011. Building and destroying continental mantle. Annu. Rev. Earth Planet. Sci. 39, 59–90.

Li, T., Jiang, M., Zhao, L., Yao, W., Chen, L., Chu, Y., Sun, B., Ai, Y., Wan, B., Gessner, K., Yuan, H., 2022. Wedge tectonics in South China: constraints from new seismic data. Sci. Bull.

Li, X.-Y., Zheng, J.-P., Xiong, Q., Zhou, X., Xiang, L., 2018. Triassic rejuvenation of unexposed Archean-Paleoproterozoic deep crust beneath the western Cathaysia block, South China. Tectonophysics 724–725, 65–79.

Li, X.H., Li, Z.X., Li, W.X., 2014. Detrital zircon U–Pb age and Hf isotope constrains on the generation and reworking of Precambrian continental crust in the Cathaysia Block, South China: a synthesis. Gondwana Res. 25, 1202–1215.

Li, Z.X., Li, X.H., Zhou, H., Kinny, P.D., 2002. Grenvillian continental collision in south China: new SHRIMP U-Pb zircon results and implications for the configuration of Rodinia. Geology 30, 163–166.

Liu, H., Chen, F., Leng, W., Zhang, H., 2017. Crustal footprint of the Hainan plume beneath southeast China. J. Geophys. Res. 123, 3065–3079.

Ma, R.S., 2006. New thoughts about the tectonic evolution of South China and discussion on a number of issues related to the so-called "Cathaysian old land". Geol. J. China Univ. 12, 448–456. in Chinese.

Mitchell, B.J., 1995. Anelastic structure and evolution of the continental crust and upper mantle from seismic surface wave attenuation. Rev. Geophys. 33, 441–462.

Mitchell, B.J., Hwang, H.J., 1987. Effect of low-Q sediments and crustal Q on Lg attenuation in the United States. Bull. Seismol. Soc. Am. 77, 1197–1210.

Morgan, J.V., Christeson, G.L., Zelt, C.A., 2002. Testing the resolution of a 3D velocity tomogram across the Chicxulub crater. Tectonophysics 355, 215–226.

Paige, C.C., Saunders, M.A., 1982. LSQR an algorithm for sparse linear-equations and sparse least-squares. ACM Trans. Math. Softw. 8, 43–71.

Paul, J., Ghosh, A., 2019. Evolution of cratons through the ages: a time-dependent study. Earth Planet. Sci. Lett. 531, 115962.

Phillips, W.S., Hartse, H.E., Rutledge, J.T., 2005. Amplitude ratio tomography for regional phase Q. Geophys. Res. Lett. 32.

Ringdal, F., Marshall, P.D., Alewine, R.W., 1992. Seismic yield determination of Soviet underground nuclear-explosions at the Shagan river test site. Geophys. J. Int. 109, 65–77.

Sato, H., Fehler, M.C., Maeda, T., 2012. Seismic Wave Propagation and Scattering in the Heterogeneous Earth, second edition. Springer, Berlin, Heidelberg.

Shu, L., Yao, J., Wang, B., Faure, M., Charvet, J., Chen, Y., 2021. Neoproterozoic plate tectonic process and Phanerozoic geodynamic evolution of the South China Block. Earth-Sci. Rev. 216, 103596.

Shu, L.S., 2006. Predevonian tectonic evolution of South China: from Cathaysian block to Caledonian period folded orogenic belt. Geol. J. China Univ. 12, 418–431. in Chinese.

Sun, Y., Dong, S., Zhang, H., Li, H., Shi, Y., 2013. 3D thermal structure of the continental lithosphere beneath China and adjacent regions. J. Asian Earth Sci. 62, 697–704.

Tapponnier, P., Molnar, P., 1976. Slip-line field-theory and large-scale continental tectonics. Nature 264, 319–324.

Wang, K., Li, Z.-X., Dong, S., Cui, J., Han, B., Zheng, T., Xu, Y., 2018. Early crustal evolution of the Yangtze Craton, South China: new constraints from zircon U-Pb-Hf isotopes and geochemistry of ca. 2.9–2.6 Ga granitic rocks in the Zhongxiang complex. Precambrian Res. 314, 325–352.

Wang, M., Shen, Z.K., 2020. Present-day crustal deformation of continental China derived from GPS and its tectonic implications. J. Geophys. Res. 125.

Wang, Y., Zhang, Y., Fan, W., Geng, H., Zou, H., Bi, X., 2014. Early Neoproterozoic accretionary assemblage in the Cathaysia Block: geochronological, Lu–Hf isotopic and geochemical evidence from granitoid gneisses. Precambrian Res. 249, 144–161.

Wang, Y.J., Fan, W.M., Zhang, G.W., Zhang, Y.H., 2013. Phanerozoic tectonics of the South China Block: key observations and controversies. Gondwana Res. 23, 1273–1305.

Wu, R.S., Jin, S.W., Xie, X.B., 2000. Energy partition and attenuation of Lg waves by numerical simulations using screen propagators. Phys. Earth Planet. Inter. 120, 227–243.

Xu, X.S., O'Reilly, S.Y., Griffin, W.L., Deng, P., Pearson, N.J., 2005. Relict proterozoic basement in the Nanling Mountains (SE China) and its tectonothermal overprinting. Tectonics 24, TC2003.

Yao, J., Cawood, P.A., Shu, L., Zhao, G., 2019. Jiangnan Orogen, South China: a ~970–820 Ma Rodinia margin accretionary belt. Earth-Sci. Rev. 196, 102872.

Yao, J., Shu, L., Cawood, P.A., Li, J., 2017. Constraining timing and tectonic implications of Neoproterozoic metamorphic event in the Cathaysia Block, South China. Precambrian Res. 293, 1–12.

Ye, T., Huang, C., Deng, Z., 2017. Spatial database of 1:2500000 digital geologic map of People's Republic of China. Geol. China 44, 24–31.

Yin, Y., Jin, S., Wei, W., Lü, Q., Ye, G., Jing, J.e., Zhang, L., Dong, H., Xie, C., 2021. Lithosphere structure and its implications for the metallogenesis of the Nanling Range, South China: constraints from 3-D magnetotelluric imaging. Ore Geol. Rev. 131, 104064.

Yu, J.H., O'Reilly, S.Y., Wang, L.J., Griffin, W.L., Zhou, M.F., Zhang, M., Shu, L.S., 2010. Components and episodic growth of Precambrian crust in the Cathaysia Block, South China: evidence from U-Pb ages and Hf isotopes of zircons in Neoproterozoic sediments. Precambrian Res. 181, 97–114.

Yu, J.H., Wang, L.J., O'Reilly, S.Y., Griffin, W.L., Zhang, M., Li, C.Z., Shu, L.S., 2009. A Paleoproterozoic orogeny recorded in a long-lived cratonic remnant (Wuyishan terrane), eastern Cathaysia Block, China. Precambrian Res. 174, 347–363.

Zhang, J., Wang, B.Y., Tang, X.C., Dong, M., Ai, Y.F., 2018. Temperature structure and dynamic background of crust and mantle beneath the high heat flow area of the South China continental margin. Chin. J. Geophys. 61, 3917–3932. in Chinese.

Zhang, K., Lü, Q., Zhao, J., Hu, H., Luo, F., Fu, G., Tao, X., 2020. Magnetotelluric evidence for the multi-microcontinental composition of eastern South China and its tectonic evolution. Sci. Rep. 10, 13105.

Zhang, L.T., Jin, S., Wei, W.B., Ye, G.F., Jing, J.N., Dong, H., Xie, C.L., 2015. Lithospheric electrical structure of South China imaged by magnetotelluric data and its tectonic implications. J. Asian Earth Sci. 98, 178–187.

Zhang, S.B., Zheng, Y.F., 2013. Formation and evolution of Precambrian continental lithosphere in South China. Gondwana Res. 23, 1241–1260.

Zhang, T.R., Lay, T., 1995. Why the Lg phase does not traverse oceanic crust. Bull. Seismol. Soc. Am. 85, 1665–1678.

Zhang, Z.J., Xu, T., Zhao, B., Badal, J., 2013. Systematic variations in seismic velocity and reflection in the crust of Cathaysia: new constraints on intraplate orogeny in the South China continent. Gondwana Res. 24, 902–917.

Zhao, G.C., Cawood, P.A., 2012. Precambrian geology of China. Precambrian Res. 222–223, 13–54.

Zhao, L.-F., Xie, X.-B., He, J.-K., Tian, X., Yao, Z.-X., 2013. Crustal flow pattern beneath the Tibetan Plateau constrained by regional Lg-wave Q tomography. Earth Planet. Sci. Lett. 383, 113–122.

Zhao, L.F., Xie, X.B., 2016. Strong Lg-wave attenuation in the Middle East continental collision orogenic belt. Tectonophysics 674, 135–146.

Zheng, J.P., Griffin, W.L., Li, L.S., O'Reilly, S.Y., Pearson, N.J., Tang, H.Y., Liu, G.L., Zhao, J.H., Yu, C.M., Su, Y.P., 2011. Highly evolved Archean basement beneath the western Cathaysia Block, South China. Geochim. Cosmochim. Acta 75, 242–255.

Zheng, J.P., Griffin, W.L., O'Reilly, S.Y., Zhang, M., Pearson, N., Pan, Y.M., 2006. Widespread Archean basement beneath the Yangtze craton. Geology 34, 417–420.

Zhou, L.Q., Xie, J.Y., Shen, W.S., Zheng, Y., Yang, Y.J., Shi, H.X., Ritzwoller, M.H., 2012. The structure of the crust and uppermost mantle beneath South China from ambient noise and earthquake tomography. Geophys. J. Int. 189, 1565–1583.

Zhu, R., Zhao, G., Xiao, W., Chen, L., Tang, Y., 2021. Origin, accretion, and reworking of continents. Rev. Geophys. 59, e2019RG000689.